Journal of Materials Chemistry A

Accepted Manuscript

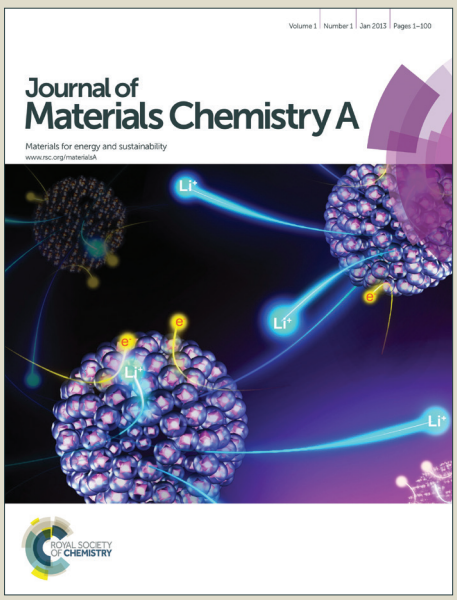

ROYAL SOCIETY OF CHEMISTRY

www.rsc.org/materialsA

Journal of Materials Chemistry A

ARTICLE

Synthesis of Nanocomposite with Carbon-SnO_2 Dual-shells on TiO_2 Nanotubes and Application in Lithium Ion Batteries

Received 00th January 20xx,
Accepted 00th January 20xx

DOI: 10.1039/x0xx00000x

www.rsc.org/

Zhongtao Li, Yuankun Wang, Hongdi Sun, Wenting Wu, Mei Liu, Jingyan Zhou, Guiliang Wu and Mingbo Wu*

Through the introduction of well-distributed tin oxide nanocrystals on the surface of pre-prepared TiO_2 nanotubes and followed by carbon coating, a novel TiO_2 / SnO_2-C double-shells nanotube has been synthesized. As an anode material of Li-ion batteries (LIBs), DSNTs exhibit excellent long-term cycling stability (256.0 $mAh{\cdot}g^{-1}$ at 1 $A{\cdot}g^{-1}$, negligible capacity decay after 710 cycles) and satisfactory rate capability, which are ascribed to the synergetic effects of a unique combination of material properties in the well-designed conductive matrix: high volume stable titanium dioxide to form one-dimensional (1D) core section to maintain the structures, large theoretical capacity tin oxide as functional layer to increase capacity and high conductive carbon as buffer layer to accelerate charging rate.

1. Introduction

The design and synthesis of high capacity and long lifespan lithium batteries (LIBs) are urgently needed to meet the increasing requirement in the field of portable devices, electrical vehicles and hybrid electric vehicles.[1-3] Currently, commercial lithium-ion batteries predominantly use graphite as anode materials, which suffers low capacity and somewhat safety issues, which due to the growth of lithium dendrites during discharge/charge cycling at a low Li-intercalation potential.[4] To further improve the performance of LIBs, numerous efforts have been undertaken toward using metal oxides (M_xO_y, M=Sn, Zn, Co, etc) alternatives, which have high theoretical capacities compared to carbonaceous materials.[5-8] Unfortunately, the reversible charging/discharging process of most of these materials involves tremendous volume variation and dramatic mechanical stress, which leads to electrode disintegration (electrochemical pulverization) and rapid capacity fading.[3,21]

Among these metal oxides materials, TiO_2 is one excellent candidate for anode material due to its low cost, eco-friendliness and particularly negligible volume expansion during the discharge-charge process, which lead to long cycle life and durability.[9] Moreover, TiO_2 exhibits a high operating voltage (>1.5 V vs Li^+/Li) to avoid the growth of lithium dendrites and improve LIBs safety.[10] Although TiO_2 are so attractive because of these advantages, their commercial use is still hindered. The critical problems are the poor electronic conductivity, low Li-ion diffusion ability, and intrinsically low theoretical capacity.[11,31] To overcome these problems, TiO_2 particles with various nanostructure and morphology have been developed to improve their performances, such as nanoparticles, nanowires, nanosheets and nanotubes etc.[12-15] Although, the electrochemistry properties of these nano-materials have been obviously improved, most of their capacities are still too low to practically apply (less than 200 $mAh{\cdot}g^{-1}$ at 1 $A{\cdot}g^{-1}$).

To further increase the capacity of titania-based materials for LIBs anode, combined TiO_2 with high conductive and theoretical capacity materials are very available ways, such as carbon and SnO_2.[16,17] While SnO_2 in composite electrodes can contribute to maintain the high capacity, TiO_2 can accommodate the volume expansion and maintain the structural integrity of the electrodes, the high conductive carbon coating on surface could improve the composites' electronic conductivity. Considering that carbon, TiO_2 and SnO_2 materials possess complementary characteristics in LIBs, numerous strategies have been developed in the recent years to design composite nanostructured TiO_2–SnO_2-C ternary systems.[18] For instance, Li and co-workers reported mesoporous TiO_2-Sn/C core-shell microspheres with superior cycling stability and high rate performance.[19] Chen group have synthesized a new nanostructure of SnO_2 nanoparticles (NPs) encapsulated into hollow TiO_2 nanowires with reversible capacity of 445mAh.g^{-1} at 800mA.g^{-1}.[26]

Even various TiO_2/SnO_2 composites with 1D nanostructure have been reported, few of which chose TiO_2 nanotubes as building block for material preparation.[17,26] The nanotubes with hollow interior could provide extra voids to effectively alleviate the volume change and mechanical strain derived from the repeated Li^+ insertion/ extraction process. More importantly, the larger specific surface area of nanotubular

State Key Laboratory of Heavy Oil Processing, China University of Petroleum, Qingdao 266580, China; *E-mail: wumb@upc.edu.cn; Fax: +86532-86984615; Tel: +86532-86984615*

Electronic Supplementary Information (ESI) available: TGA and EDS data of the DSNTs, full range of the XPS spectrum, discharge-charge profiles of TiO_2, TiO_2-C and TiO_2-SnO_2. See DOI: 10.1039/x0xx00000x

materials could afford more reactive sites for electrode-electrolyte and accelerate electrons and ions transportation. In the last, when coated by high conductive carbon on the surface of 1D nanotube with large length/diameter ratio, the composites could be effectively cross-linked with each other to fabricate conductive matrix.[20]

Herein, we report the synthesis of TiO_2-SnO_2/C double-shell nanotubes (namely DSNTs) via two hydrothermal processes and followed by one liquid phase reaction proces. Urea is introduce into the reaction as surfactant and pH regulator in the hydrothermal process to well-disperse tin oxide particles in nanoscale, which could be adhered firmly on the surface of titanium dioxide. To prevent the aggregation of SnO_2 into large grains and to buffer volume change and structural stress, resorcinol-formaldehyde (RF) is adopted as carbon source to form a highly electric conductive coating on TiO_2-SnO_2 nanostructure. The unique Ti-Sn-C ternary double-shell nanostructure not only provides a large interfacial area for fast lithium insertion/extraction but also reduces the diffusion pathways for electronic and ionic transport. The as-fabricated electrodes show several desirable electrochemical features: high specific capacity, excellent cycle stability, and good rate capability, which reveal a potential way to practical applying TiO_2 for next-generation LIBs.

2. Experimental Section

2.1. Preparation of TiO_2 nanotubes

Preparation of TiO_2 nanotubes: TiO_2 nanotubes were prepared according to previous reports with slightly modifications.[22,23] In a typical synthesis, 0.4 g commercial TiO_2 was firstly dispersed into 60 mL of aqueous solution with the aid of ultrasonic. Then, 24 g NaOH was added, and the solutions were transferred into Teflon-lined stainless steel autoclave with a magnetic stirrer. The autoclave was put in silicon oil bath on a hot plate and reacted 150 °C for 24 h. The stirring rate was set at ~300 rpm. Then, the autoclave was taken out from oil bath and naturally cooled to room temperature. The white precipitates were collected by centrifugation, washed with deionized water and 0.1 M HNO_3 solution for several times to obtain $H_2Ti_2O_5{\cdot}H_2O$ tubes. Then, the $H_2Ti_2O_5{\cdot}H_2O$ was washed with DI water for several times until a pH value of 7 was reached, and dried in the oven overnight for the following thermal teartment. Finally, the TiO_2 nanotubes were obtained after heat up dried $H_2Ti_2O_5{\cdot}H_2O$ in a tube furnace to 500 °C for 2 h in air.

2.2. Preparation of TiO_2-SnO_2 core-shell nanotubes

In a 200 mL beaker, 1.8 g (30 mmoL) urea, 240 mg as-prepared TiO_2 nanotubes, and 0.212 g (1 mmoL) Na_2SnO_3 were mixed with 38 mL DI water and 18 mL ethanol by ultrasonication to form a milky white suspension. After ultrasonic for 30 min, the suspension was transferred into Teflon-lined stainless steel autoclave and kept at 180 °C for 18 h. After cooled to room temperature, the TiO_2-SnO_2 core-shell nanotubes were collected by centrifugation, and washed with deionized water for several times and dried in oven.

2.3. Preparation of TiO_2-SnO_2/C double-shells nanotubes and TiO_2-C core-shell nanotubes

200 mg TiO_2-SnO_2 core-shell nanotubes was sequentially mixed with 145 mL of distilled water, 10 mL of cetyltrimethylammonium bromide (CTAB) aqueous solution (0.01M), 1.0 mL of ammonia aqueous solution (28 wt %), 100 mg of resorcinol, and 280 µL of formaldehyde at 50 °C. After reaction of 1 h at 50 °C, the solid product was collected by centrifugation, washed with water and ethanol, and air-dried at 80 °C for several hours. The as prepared TiO_2-SnO_2/C composites were finally calcined under an argon atmosphere at 500 °C for 2 h.

To further understand the function of RF coating, TiO_2-C core-shell nanotubes was prepared as a control sample. In this section, TiO_2 nanotubes are adopted as starting material and coated by the RF through the same processes as mentioned above.

2.4. Sample characterization

The phase purity and crystal structure of the samples was characterized by X-ray powder diffraction (XRD) using an X-ray diffractometer with Cu Kα radiation from 10-75°. Transmission electron microscopy (TEM, JEM-2100UHR, Japan, equipped with energy dispersive X-ray spectroscopy (EDS)) and high-resolution transmission electron microscopy (HRTEM) were used to examine the morphologies, crystalline structures and element distributions of the samples. The Raman spectra were measured on a Renishaw DXR Raman spectros system with a 532 nm laster source. The elemental valences of the samples were analyzed by using X-ray photoelectron spectroscopy (XPS, Thermo Scientific ESCALab250Xi).

2.5. Electrochemical measurement

The working electrodes were prepared by coating the slurry of the as-prepared samples, carbon black and poly(vinylidene) fluoride (PVDF) binder (80: 10: 10 in weight ratio) dissolved in N-methyl-2-pyrrolidinone (NMP) onto a copper foil current collector. After coating, the prepared working electrode was dried at 100 °C for 10 h. The electrodes were cut to disks typically with a diameter of ~12 mm, and the active materials average mass loading within the coin cells are around 1.3 mg for TiO_2, 1.3 mg for TiO_2-C, 1.7 mg for TiO_2-SnO_2, and 1.5 mg for DSNTs. Li foil was used as the counter electrode and the reference electrode. The electrolyte was LiPF6 (1 mol L^{-1}) dissolved in a mixture of dimethyl carbonate (DMC) and ethylene carbonate (EC) with a volume ratio of 1:1. The galvanostatic method at the different charge/discharge current densities from 0.5 $A{\cdot}g^{-1}$ to 5 $A{\cdot}g^{-1}$ was employed to measure the electrochemical capacity and cycle life of the electrode at room temperature using a LAND-CT2001A cycler. Cyclic voltammograms (CV) were performed using an Ametek

PARSTAT4000 electrochemistry workstation at 0.2 mV s^{-1} within the potential range of 0.005–2.5 V.

3. Results and discussion

Fig. 1 illustrates the whole process of DSNTs, which involves three steps. Firstly, anatase TiO_2 nanotubes were synthesized by a high-temperature hydrolysis reaction and ion exchange with HNO_3, followed by calcination. Then, the outer surface of the TiO_2 nanotubes was coated with a thin layer of SnO_2 nanoparticle by another hydrothermal treatment. Finally, the as-obtained TiO_2-SnO_2 nanotubes were coated with resorcinol-formaldehyde (RF) through a solution process by reacting resorcinol with formaldehyde in the presence of ammonia and CTAB, and calcination at 500 °C to induce the carbonization of the cross-linked polymer.

The structural characteristics of the as-prepared TiO_2, TiO_2-SnO_2, and DSNTs were determined by XRD (Fig. 2). As shown in Fig. 2a, all pronounced peaks can be indexed to the anatase TiO_2 (JCPDS card no. 21-1272, a=b=3.785 Å, c=9.514 Å) with high crystallinity. In Figure 2b, the XRD profile of the TiO_2-SnO_2 nanotubes indicates the presence of both anatase TiO_2 and cassiterite SnO_2 phases in the sample. The diffraction peaks at 26.6°, 33.9°, 37.9°, 51.8°,and 65.9° correspond well to the (110), (101), (200), (211), and (301) planes of cassiterite SnO_2 (JCPDS card no. 41-1445, a=4.738 Å, b=4.738 Å, c= 3.187 Å).

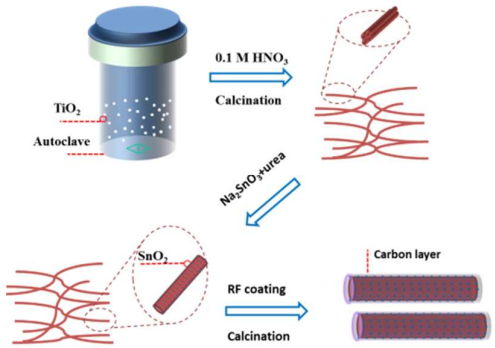

Fig. 1 Schematic illustration of the fabrication process.

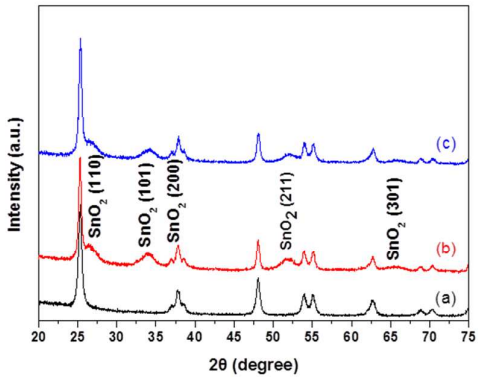

Fig. 2 XRD patterns of as-prepared (a) TiO_2 nanotubes, (b) TiO_2-SnO_2 core-shell nanotubes, and (c) DSNTs.

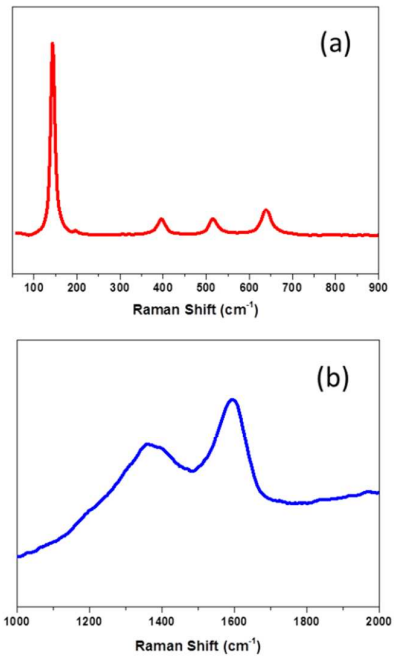

Fig. 3 Raman spectrum of (a) TiO_2 nanotubes, (b) DSNTs

The SnO_2 peaks in Fig. 2b and 2c are broad and low, which indicates that SnO_2 nanoparticles (NPs) are very small and not well crystallized in the composites. The mean particle size of the SnO_2 was calculated using Scherrer's formula as 7 nm. After RF coating and carbonization process, the XRD data of the final product was not changed (Fig. 2c).

To further understand the product properties, Raman spectra of TiO_2 nanotubes and DSNTs in Fig. 3a were carried out. The peaks at 143, 400, 515, and 637 cm^{-1} are indicated the characteristic of the anatase TiO_2 in TiO_2 nanotubes, which is consistent with the results of XRD analysis. Moreover, the characteristic D band at ~1350 cm^{-1} and G band at ~1590 cm^{-1} are observed for the DSNTs, the intensity of the G-band is high than that of the D-bands (I_D/I_G ratio of 0.85) which revealed the good graphitization of the carbon layer after heat treatment at 500 °C for 2h in N_2.

To assess the thermal properties and the compositions of DSNTs, thermogravimetric analysis (TGA) was carried out in air. As shown in Fig. S1, the major mass loss occurred in the range of 200-600 °C can be ascribed to the combustion of carbon coating in air. Finally, the curve of SnO_2-QDs/N-GNs tends to be horizontal; we can deduce that the carbon content is about 10.0%.

To further investigate the chemical composition and valence states of the DSNTs, XPS spectra and EDS data were tested. The experiment data indicated that the DSNTs are composed of C, O, Ti, and Sn. The EDS data (Fig. S2) revealed the percentages of tin and titanium in DSNTs are 1.94 at% and 9.25 at%, respectively. But the elements content of Sn and Ti are 3.23 at% and 6.16 at% as shown in XPS data in Fig. S3. The higher content of tin in XPS data is due to that the distribution

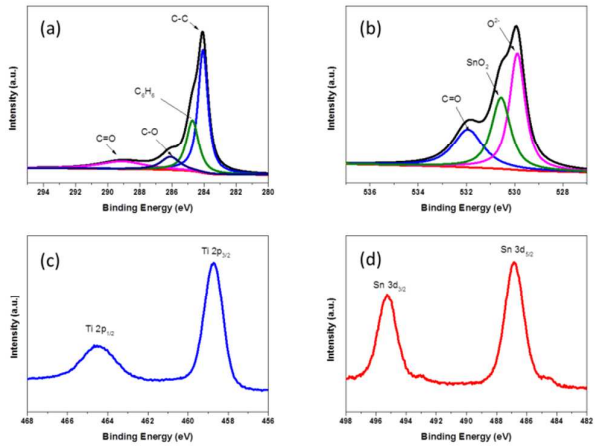

Fig. 4 XPS spectra of (a) C 1s, (b) O 1s, (c) Ti 2p and (d) Sn 3d regions of DSNTs.

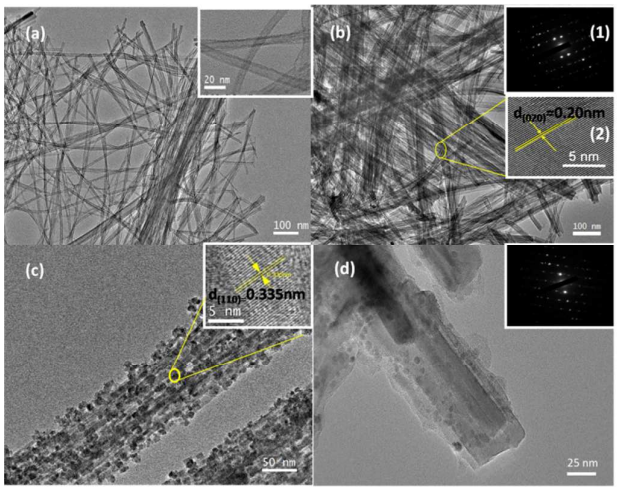

Fig. 5 (a-d) Low-magnification TEM images of $H_2Ti_2O_5·H_2O$ nanotubes, TiO_2 nanotubes, TiO_2-SnO_2 nanotubes, and DSNTs, respectively; inset in (a), (b (2)), and (c) are high-magnification TEM images for $H_2Ti_2O_5·H_2O$ nanotubes, TiO_2 nanotubes, and TiO_2-SnO_2 nanotubes respectively; inset in (b (1)) and (d) are SAED patterns of TiO_2 nanotubes and DSNTs, respectively.

of most tin oxide are on the surface of nanotubes. In Fig. 4, the XPS results reveal C, O, Ti, and Sn spectra in DSNTS. The high resolution C 1s spectrum (Fig. 4a) was centered at 284.1 eV, which can be well identified into four components at binding energies of 284.1 eV (non-oxygenated carbon (C-C)), 284.7 eV (C_6H_6), 286.1 eV (C-O-C/ C-OH), and 289.17 eV (carbonyl group (C=O)), respectively.[24] The deconvoluted peaks (Fig. 4b) of the O 1s spectrum were resolved into three components, centered at 529.9, 530.5, and 531.9 eV, respectively. The binding energy component observed at 529.9 eV and 530.5 eV are attributed to auger electron of O^{2-} in TiO_2 and SnO_2, while, the peak at 531.9 eV can be assigned to C=O bonds in carbonyl group. Fig. 4c exhibits the Ti 2p XPS spectrum, in which two distinct peaks at 464.7 eV and 458.7 eV can be assigned to Ti $2p_{1/2}$ and Ti $2p_{3/2}$ respectively, which reflect a typical signal of Ti^{4+} in octahedral crystal.[25] The curve fitted core level spectra of Sn 3d are shown in Fig. 4d. Two peaks at 495.3 eV and 486.8 eV could be found, which correspond well to the Sn $3d_{3/2}$ and Sn $3d_{5/2}$ and demonstrate the formation of SnO_2.[27]

As shown in Fig. 5, the morphologies and nanostructures of the as-prepared composites were characterized by TEM. In Fig. 5a, elongated $H_2Ti_2O_5·H_2O$ nanotube was formed by mechanical force driven during hydrothermal process, which are around 10 nm in diameter and 4.5 μm in length on average. After the first high temperature calcination, the crystalline nanotubes were transferred from $H_2Ti_2O_5·H_2O$ to anatase TiO_2 through a topotactic transformation.[25] In addition, the diameter of the nanotubes also increase after thermal annealing due to the merging of parallel orientated multiple nanotubes, as can be seen from Fig. 5b.[23] In the high resolution TEM image, a lattice spacing of 0.20 nm could be defined, which can be ascribed to the (020) planes of anatase TiO_2 (Fig. 5b(2)). The selected area electron diffraction (SAED) pattern of the TiO_2 nanotube (Fig. 5b(1)) shows a set of well-defined dots, indicative of single-crystallinity anatase TiO_2. The results of HR-TEM and SAED affirm that the nanotubes prefer to grown in the (010) crystallographic direction, consistent with the findings in a previous study.[22] Fig. 5b shows the TEM images of the TiO_2-SnO_2 nanotubes. The roughness of TiO_2-SnO_2 nanotubes is increased, which indicates the successful deposition of SnO_2 nanoparticles on TiO_2 nanotubes, which also have been confirmed by Brunaeuer-Emmett-Teller (BET) N_2 adsorption-desorption analysis (Fig. S4). The experiment data revealed that the specific surface area of TiO_2-SnO_2 is increase to 94.75 $m^2 g^{-1}$, which is 67.35 $m^2.g^{-1}$ of pure TiO_2 tubes. The average diameter of the SnO_2 nanoparticles is approximate 7 nm, which have been approved by XRD. The lattice fringes of SnO_2 nanoparticles is measured as 0.335 nm, which is in agreement with the d-spacing of the (110) plane of cassiterite SnO_2, as shown in the inset of Fig. 5c. After solution process with RF and carbonization in Ar, a well carbon coating could be identified in the core-shell structure (Fig. 5d). The coated carbon layer that around 10 nm in thick, is uniformly covered on the surface of TiO_2-SnO_2 nanotubes.[20] In addition, SAED patterns were recorded by focusing the electron beam on an area indicated by a square (inset of Fig. 5d), indicating the cassiterite SnO_2 and anatase TiO_2 are both existed in DSNTs.

The experiment data of discharge-charge measurements of the DSNTs are shown in Fig. 6. Discharge-charge measurements were carried out at a current density of 500 $mA·g^{-1}$ between 0.005 to 2.5 V (vs. Li) at room temperature. The voltage versus capacity profiles are shown in Fig. 6a. In the discharge curve of the first cycle, there are two obvious voltage plateaus (~1.7 and 0.74 V) resulting from the lithium reactions with TiO_2 and SnO_2, respectively. The first plateau at ~1.7 V is associated with the phase transition between the tetragonal TiO_2 and orthorhombic Li_xTiO_2 phase.[28,29] The second plateau at 0.74 V can be ascribed to the reaction of SnO_2 with lithium to from the solid electrolyte interface (SEI) layers, which is not appear in the subsequent cycling.[30]

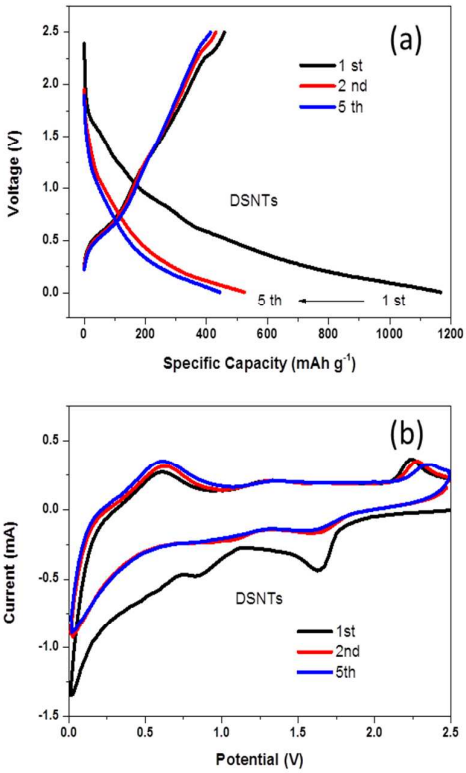

Fig. 6 (a) Discharge-charge profiles of DSNTs at a constant current density of 500 mA g^{-1}; (b) CV curves of DSNTs anode at 0.2 mV s^{-1} scanning rate

Similarly, The charge curve shows two plateau at ~0.54 and 2.1 V, which can be ascribed to the lithium extraction behaviour. The Li reaction with DSNTs electrodes can be written as:

$$TiO_2 + xLi^+ + xe^- \leftrightarrow Li_xTiO_2 \quad (0 \le x \le 1) \quad (1)$$

$$SnO_2 + 4Li^+ + 4e^- \rightarrow Sn + 2Li_2O \quad (2)$$

$$Sn + xLi + xe^- \leftrightarrow Li_xSn \quad (0 \le x \le 4.4) \quad (3)$$

Where x and x' are the amount of inserted Li^+ in anatase TiO_2 and SnO_2, respectively. The DSNTs yield a specific capacity on the first discharge (1166.6 mAh·g^{-1}) and charge (459.1 mAh·g^{-1}). The large capacity loss (~60 %) in the first cycle is mainly attributed to irreversible side reactions such as the inevitable formation of SEI film and electrolyte decomposition, which are common to most lithium intercalation hosts. The voltage-capacity trace of the TiO_2, TiO_2-C and TiO_2-SnO_2 nanotubes were also recorded for comparison (Fig. S5). In the first discharge process, the capacities gradually increase from 376.9 mAh·g^{-1} of TiO_2 to 414.8 mAh·g^{-1} of TiO_2-C, and finally to 1129.8 mAh·g^{-1} of TiO_2-SnO_2. The increased capacity can be attributed to the combination effects of RF coating and SnO_2. CV curves of DSNTs at a scan rate of 0.2 mV·s^{-1} with cut-off voltages of 2.5–0.005 V (versus Li^+/Li) are shown in Fig. 6b. In the first cycle, one pair of anatase TiO_2 cathodic/anodic peaks at 1.7 and 2.1 V can be observed, which is caused by Li insertion/extraction between TiO_2 and Li (reaction 1). Meanwhile, the irreversible cathodic peak around 0.74 V is attributed to the formation of the SEI layer, and the same voltage plateaus could be found in the discharge-charge profiles (Fig. 6a). The almost overlap curves of the second and fifth cycle indicates highly reversible redox behaviour and good cycling stability of DSNTs electrode.

Fig. 7a shows the cycling performance at a current density of 500 mA·g^{-1} for the as-prepared four materials. The discharge capacities of TiO_2, TiO_2-C, and TiO_2-SnO_2 electrodes after 120 cycles at 500 mA·g^{-1} are 76.5, 80.1, and 78.5 mAh·g^{-1}, respectively. The poor cycling stability of TiO_2-SnO_2 electrodes are due to the tremendous volume changes of SnO_2 nanoparticles.[6,30] DSNTs-based electrodes delivered improved reversible charge/discharge stability and the discharge capacity is remain 354.3 mAh·g^{-1} even after 120 cycles at a current density of 500 mA·g^{-1}. Long-term cycling performance of DSNTs at a current density of 1 A·g^{-1} is shown in Fig. 7b. The reversible discharge capacity of DSNTs electrodes after 710 cycles is 256 mAh·g^{-1}, which correspond to 85.8 % retention of the 10th discharge capacity (304.8 mAh·g^{-1}). Moreover, the columbic efficiency is almost 100 % after several cycles, which indicates high reversible of DSNTs electrodes. Such improved electrochemistry performance implying that the RF layer on the surface of the TiO_2-SnO_2 nanotubes play an essential role in accommodation of metal oxides volume change and improvement of electron conductivity. Moreover, the DSNTs also exhibit excellent rate performance as shown in Fig. 7c. Remarkably, even at a high current density of 5.0 A·g^{-1}, the capacity of this lithium-ion cell can reach around 77.0 mAh·g^{-1}. More importantly, the specific capacity rebounds back to 350.3 mAh·g^{-1} when the current density swings back to 500 mA·g^{-1}, indicating remarkable rate capability and stability of

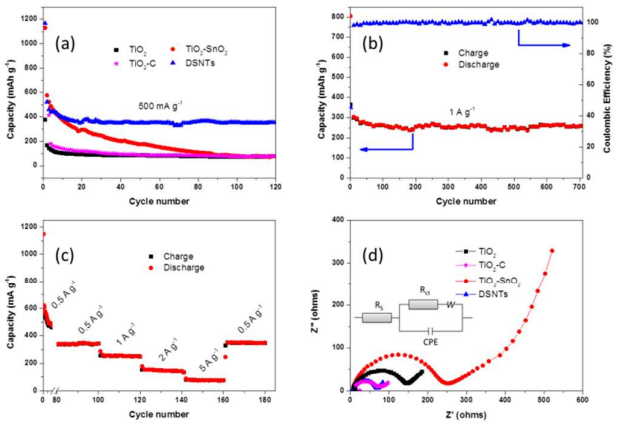

Fig. 7 (a) Cyclic performance of TiO_2, TiO_2-C, TiO_2-SnO_2, and DSNTs electrodes at a current density of 500 mA·g^{-1}, (b) long-term cycling performance of DSNTs at 1 A·g^{-1}, (c) rate capacity of DSNTs at different current densities, and (d) electrochemical impedance spectra of TiO_2, TiO_2-SnO_2 and DSNTs; the inset of (d) is the fitting circuit, R_s: ohmic resistance (total resistance of the electrolyte, separator, and electrical contacts); R_{ct}: charge transfer resistance; W: Warburg resistance; CPE: constant phase-angle element.

DSNTs. To further understanding the satisfactory electrochemical performance, a TEM image of the DSNTs after 300 cycles at 1 A g^{-1} was presented in Fig. S6. In addition to some impurities from carbon black and binder, the 1D nanotubes in DSNTs could be easily identified after long time repeated lithiation/delithiation, which indicates the excellent structure stability of DSNTs.

Fig. 7d shows the electrochemical impedance spectra (EIS) of TiO_2, TiO_2-SnO_2, and DSNTs. The Nyquist plots of all three electrodes depict a semicircle at the high-medium frequency region, corresponding to the charge transfer resistance. An inclined line at low frequency region represents the diffusion resistance. It is worth noting that the diameter of the semicircle for the DSNTs electrodes (52.34 ohm) is much smaller than that of the TiO_2 (111.1 ohm) and TiO_2-SnO_2 (212.3 ohm), which suggests that the DSNTs possess lowest contact and charge transfer resistances. It can be attributed to the fabrication of high conductive matrix through the coated nanotubes, which affords effectively channels for charge transfer through better connection with metal oxides particles.

The excellent cycling stability and rate capability of DSNTs are associated with a unique combination of material properties. In the composite, volume expansion negligible TiO_2 tubes in the core section to keep high durability and its 1D structure could effectively reduce the diffusion pathways for ionic transport; the well-defined SnO_2 nanoparticles on TiO_2 tubes could increase the lithium storage capacity. The high conductive carbon coating have the following functions: firstly, the nanotubes could connected with each other through "touching" of outer conductive carbon coating, which could effectively create a conductive network over the entire system. Secondly, the uniform carbon layer on the surface could alleviate the stress generated by large volume variation of SnO_2 NPs during the repeated cycle processes to avoid their aggregation and maintain the unique double-shell nanostructure.

4. Conclusions

In summary, TiO_2/SnO_2-C double-shells nanotubes have been synthesis for high performance Li-ion batteries anode. By introducing urea as surfactant and pH regulator during hydrothermal process, tin oxide nanocrystals are well dispersed on the surface of pre-prepared TiO_2 nanotubes. Thereafter, Resorcinol-formaldehyde (RF) is deposited on the TiO_2-SnO_2 composite and followed by thermal treatment to form a continuous carbon layer. As ascribed to the synergetic effects of a unique combination of material properties, the double-shells nanotubes exhibits a greatly enhanced reversible capacity (256 $mAh{\cdot}g^{-1}$ after 710 cycles at 1 $A{\cdot}g^{-1}$) and rate capability (77 $mA{\cdot}g^{-1}$ at 5 $A{\cdot}g^{-1}$), which are greatly improved than that of pure TiO_2, TiO_2-C, and TiO_2-SnO_2 nanotubes. The method described in this paper may provide a simple, economic and effective strategy for the preparation of next generation LIBs.

Acknowledgements

This work is supported by the National Natural Science Foundation of China (Nos. 51303212, 51303202, 21302224, 51372277); National Natural Science Foundation of Shandong Province (ZR2013BQ028, ZR2013EMQ013); The Fundamental Research Fund for the Central Universities (14CX04009A, 14CX04062A, 15CX05010A, 15CX08005A) and Open Fund of Beijing National Laboratory for Molecular Sciences (2013019).

References

1 M. V. Reddy, G. V. Subba Rao and B. V. R. Chowdari, *Chem. Rev.*, 2013, **113**, 5364.
2 W. Zhang, *J. Power Sources*, 2011, **196**, 13.
3 Z. Wang and L. Zhou, *Adv. Mater.*, 2012, **24**, 1903.
4 G. Zhu, Y. Wang and Y. Xia, *Environ. Sci. Technol.*, 2012, **5**, 6652.
5 J.S. Chen, Y.L. Cheah, Y.T. Chen, N. Jayaprakash, S. Madavi, Y.H. Yang and X.W. Lou, *J. Phys. Chem. C*, 2009, **113**, 20504.
6 Z. Li, G. Wu, D. Liu, W. Wu, B. Jiang, J. Zheng, Y. Li, J. Li and M. Wu, *J. Mater. Chem. A*, 2014, **2**, 7471.
7 S. J. Yang, S. Nam, T. Kim, J. H. Im, H. Jung, J. H. Kang, S. Wi, B. Park and C. R. Park, *J. Am. Chem. Soc.*, 2013, **135**, 7394.
8 X. W. Lou, D. Deng, J. Y. Lee, J. Feng and L. A. Archer, *Adv. Mater.*, 2008, **20**, 258.
9 W. Li, F. Wang, S. Feng, J. Wang, Z. Sun, B. Li, Y. Li, J. Yang, A. A. Elzatahry, Y. Xia and D. Zhao, *J. Am. Chem. Soc.*, 2013, **135**, 18300.
10 B. Hao, Y. Yan, X. Wang and G. Chen, *ACS Appl. Mater. Interfaces*, 2013, **5**, 6285.
11 J. Liao, D. Higgins, G. Lui, C. Victor, X. Xiao and Z. Chen, *Nanolet.*, 2013, **13**, 5467.
12 S. Bach, J. P. Pereira-Ramos and P. Willman, *Electrochim. Acta*, 2010, **55**, 4952.
13 Z. Yang, G. Du, Z. Guo, X. Yu, Z. Chen, T. Guo, N. Sharma and H. Liu, *Electrochem. Commun.*, 2011, **13**, 46.
14 S. Yang, X. Feng and K. Müllen, *Adv. Mater.*, 2011, 23, 3575.
15 J. Chen, Z. Wang, X. Dong, P. Chen and X.W. Lou, *Nanoscale*, 2011, **3**, 2158.
16 H. Wang, L. Xi, J. Tucek, C. Ma, G. Yang, M.K.H. Leung, R. Zboril, C. Niu and A.L. Rogach, *Chem. Electro. Chem*, 2014, **1**, 1563.
17 H. Wang, H. Huang, C. Niu and A. L. Rogach, *Small*, 2014, **11**, 1364.
18 J. Chen, L. Yang, Z. Zhang, S. Fang and S. Hirano, *Chem. Comm.*, 2013, **49**, 2792.
19 G. Du, Z. Guo, P. Zhang, Y. Li, M. Chen, D. Wexler and H. Liu, *J. Mater. Chem.*, 2010, **20**, 5689.
20 W. Wang, Q. Sa, J. Chen, Y. Wang, H. Jung and Y. Yin, *ACS Appl. Mater. Interfaces.*, 2013, **5**, 6478.
21 J. Liang, X. Yu, H. Zhou, H.B. Wu, S. Ding and X.W. Lou, Angew. Chem. Int. Ed. 2014, **53**, 12803.
22 Y. Tang, Y. Zhang, J. Deng, J. Wei, H.L. Tam, B. K. Chandran, Z. Dong, Z. Chen and X. Chen, *Adv. Mater.*, 2014, **26**, 6111.
23 Y. Tang, Y. Zhang, J. Deng, D. Qi, W. R. Leow, J. Wei, S. Yin, Z. Dong, R. Yazami, Z. Chen and X. Chen, *Angew. Chem. Int. Ed.*, 2014, **53**, 1.
24 Y. Luo, J. Luo, W. Zhou, X. Qi, H. Zhang, D. Y. W. Yu, C. M. Li, H. J. Fan and T. Yu, *J. Mater. Chem. A*, 2013, **1**, 273.
25 Y. Luo, J. Luo, J. Jiang, W. Zhou, H. Yang, X. Qi, H. Zhang, H. J. Fan, D.Y.W. Yu, C.M. Li and T. Yu, *Energy Environ. Sci.*, 2012, **5**, 6559.
26 H. Kim, M.G. Kim, T.J. Shin, H. S and J. Cho, *Electrochem. Commun.*, 2008, **10**, 1669.

27 Q. Tian, Z. Zhang, L. Yang and S. Hirano, *J. Power Sources,* 2014, **253**. 9.
28 H. Park, T. Song, H. Han, A. Devadoss, J. Yuh, C. Choi and U. Paik, *Electrochem. Commun.*, 2012, **22**, 81.
29 K. Saravanan, and K. Ananthanarayanan and P. Balaya, Energy Environ. Sci., 2010, **3**, 939.
30 X. Wang, Z. Li, Q. Li, C. Wang, A. Chen, Z. Zhang, R. Fan and L. Yin, CrystEngComm, 2013, **15**, 3696.
31 X. Xu, Z. Fan, S. Ding, D. Yu and Y. Du, *Nanoscale*, 2014, **6**, 5245.

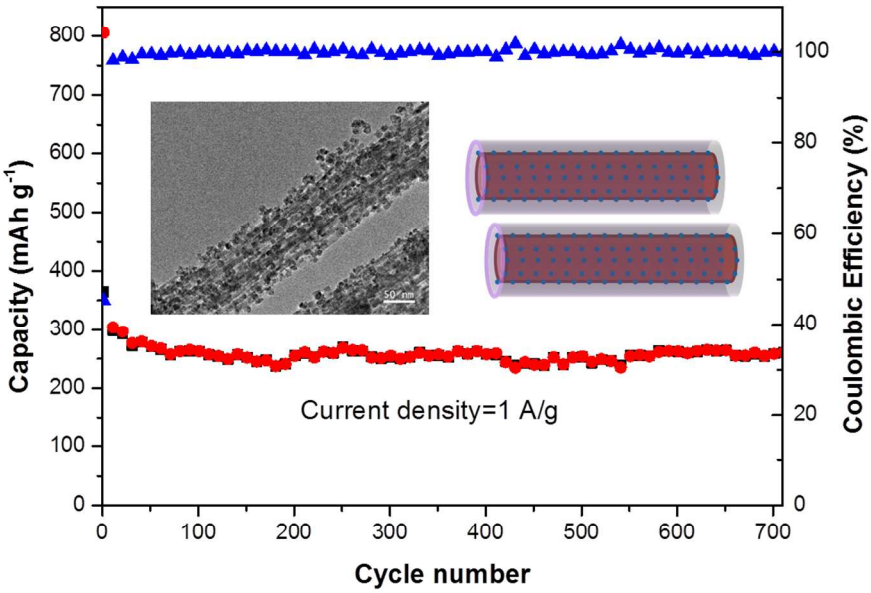

Graphical Abstract
346x242mm (96 x 96 DPI)